Electronic Supplementary Material (ESI) for Journal of Materials Chemistry A.

Supporting Information

Towards durable high performance anode material for lithium storage: stabilizing N-doped carbon encapsulated FeS nanosheets with amorphous TiO_2

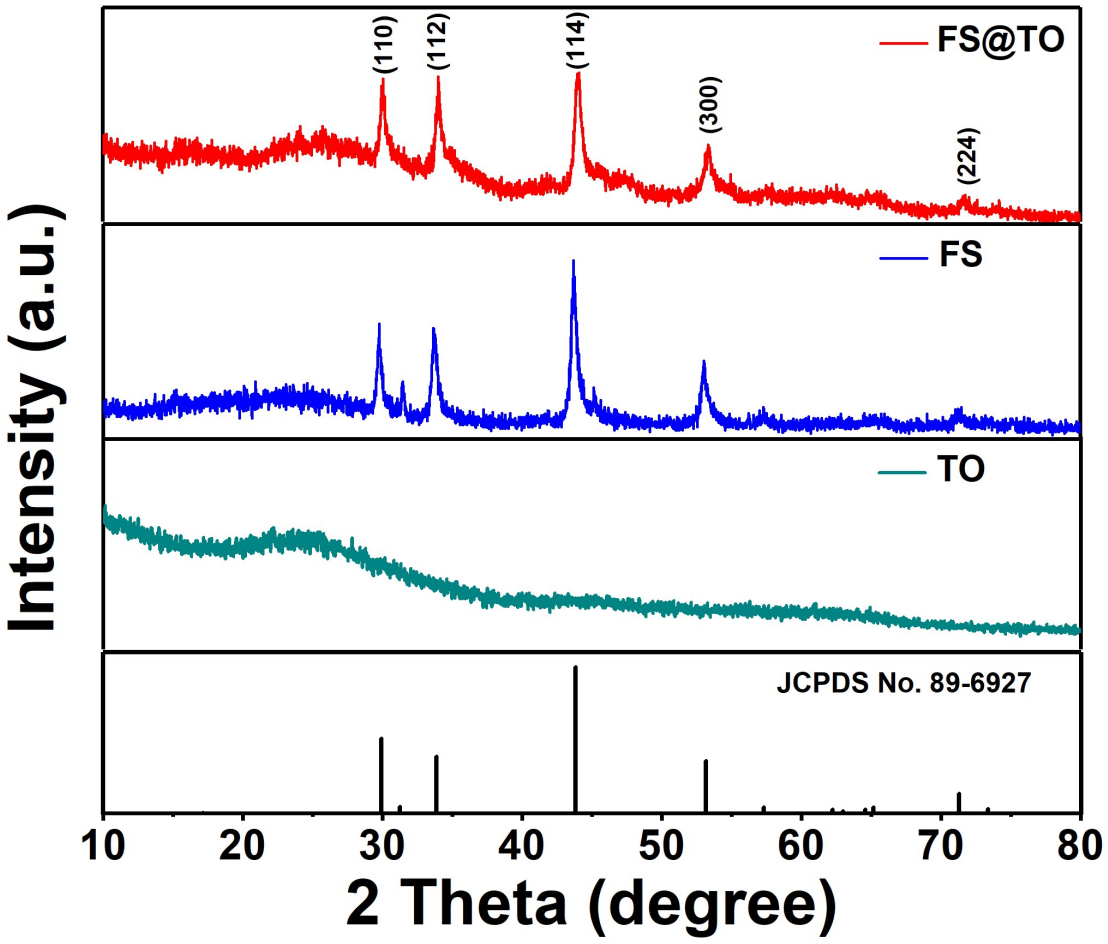

Fig. S1. X-ray diffraction patterns of FS@TO, FS and TO obtained by annealing the precursor at 500℃ for 3h.

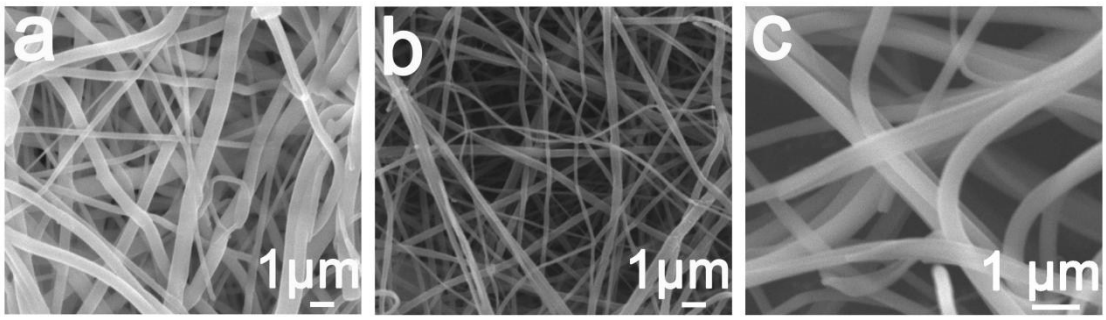

Fig. S2. (a) SEM images of the precursor of FS@TO nanofibers, (b) the precursor of FS nanofibers (c) the precursor of TO nanofibers.

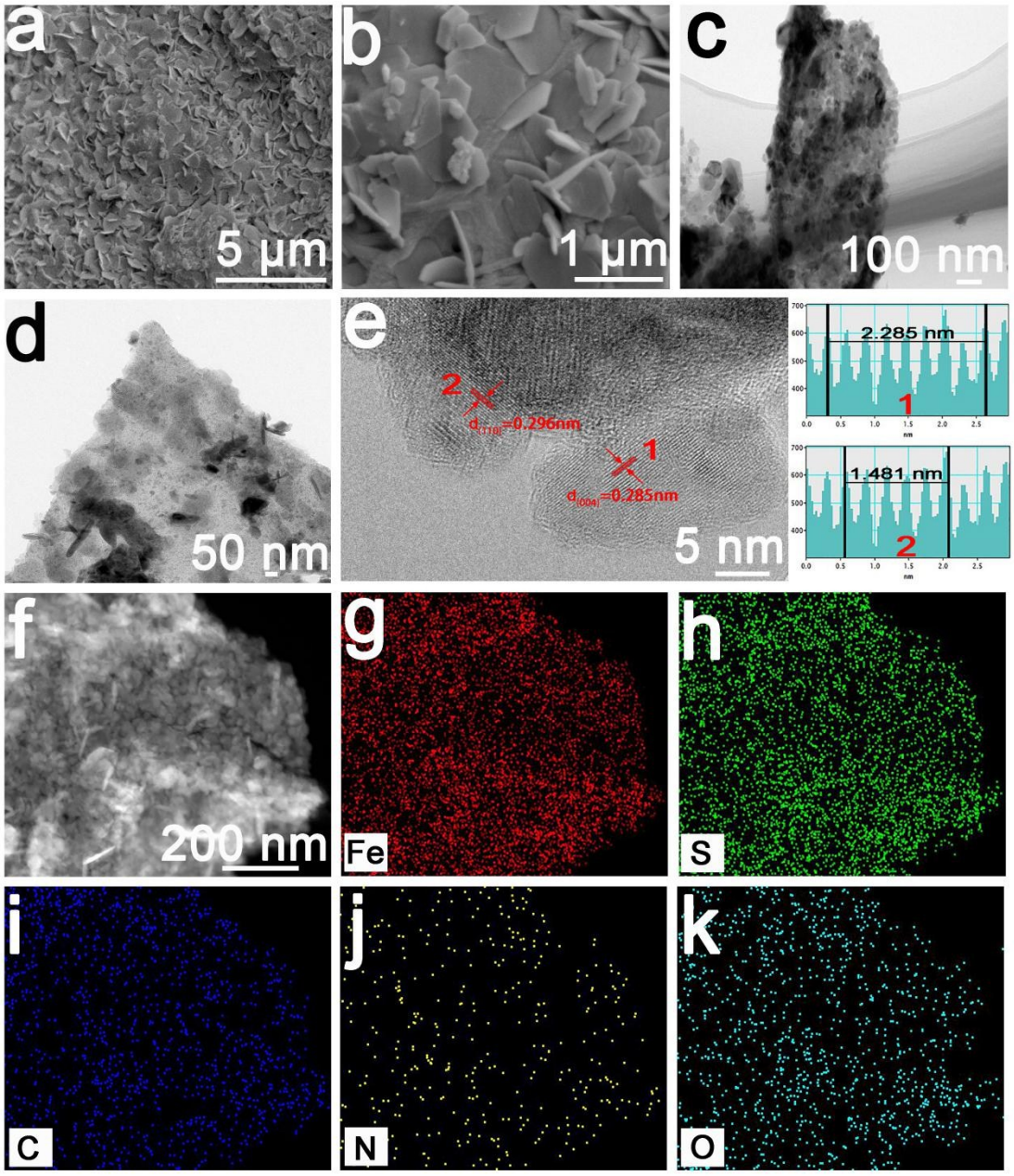

Fig. S3. (a, b) SEM images, (c, d) TEM images, (e) the high-magnification TEM images, (f-k) element mapping images (Fe, S, C, N, O) of FS nanosheets.

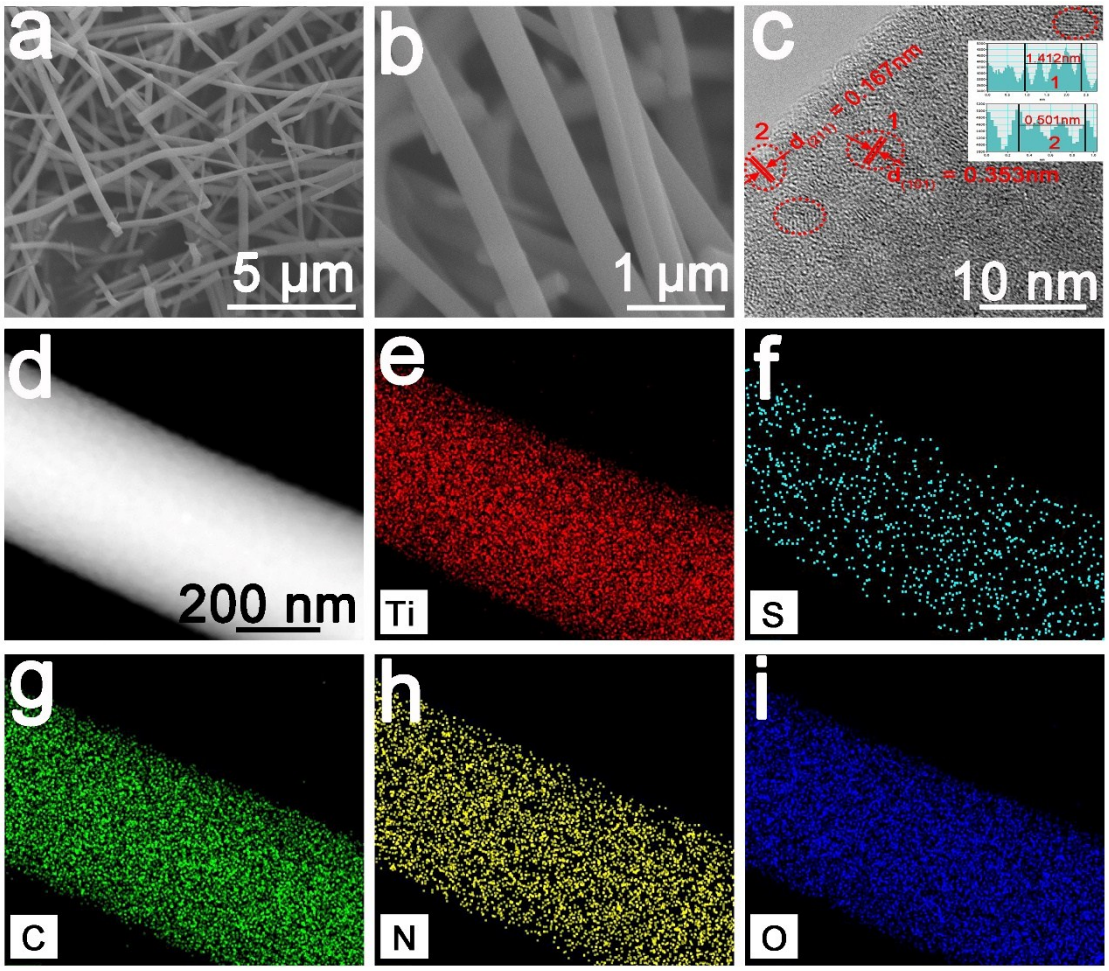

Fig. S4. (a, b) SEM images, (c) the high-magnification TEM images, (d-i) element mapping images (Ti, S, C, N, O) of TO nanofibers.

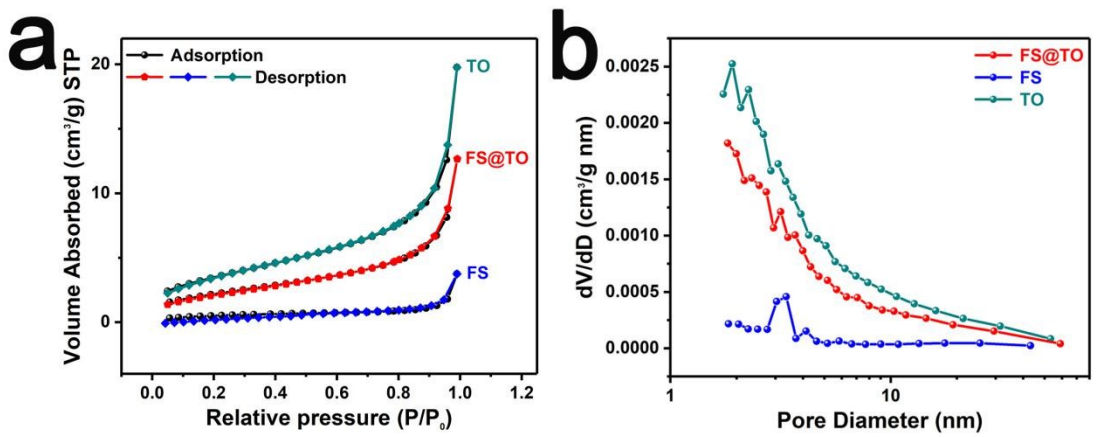

Fig. S5. (a) Nitrogen adsorption-desorption isotherms, (b) corresponding pore size distribution curves of FS@TO, FS and TO.

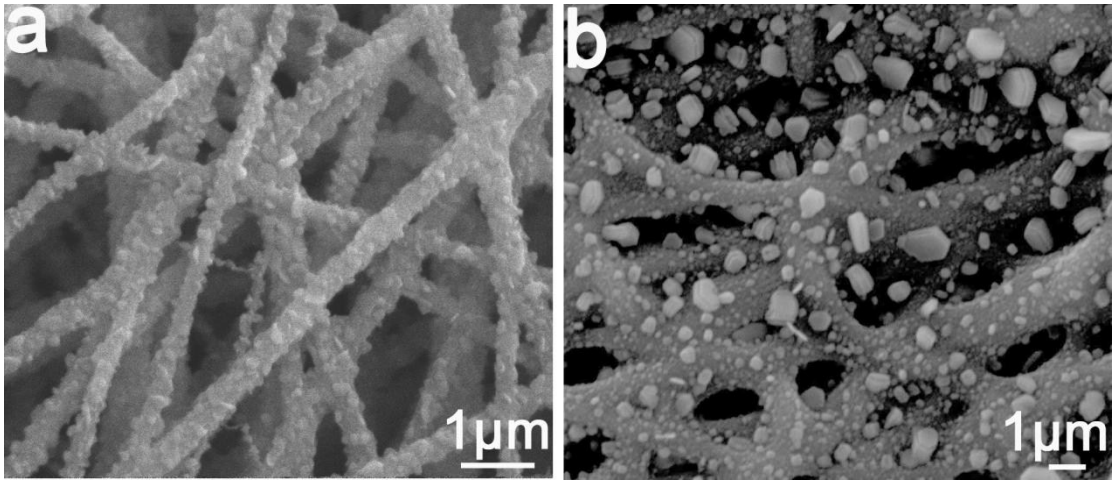

Fig. S6. (a) SEM images of FS@TO composite nanofibers at 600 ℃, (b) SEM images of FS@TO composite nanofibers at 700 ℃.

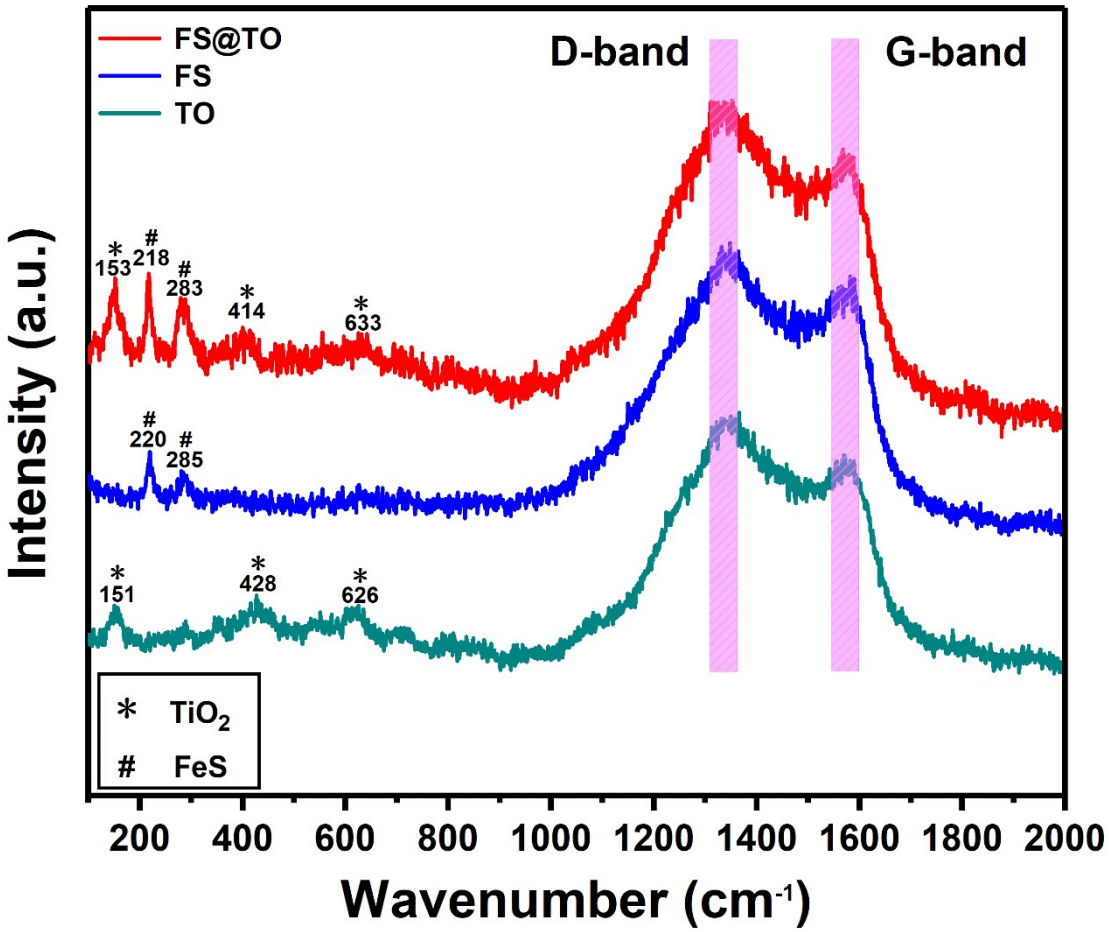

Fig. S7. Raman spectra of sample FS@TO, FS and TO.

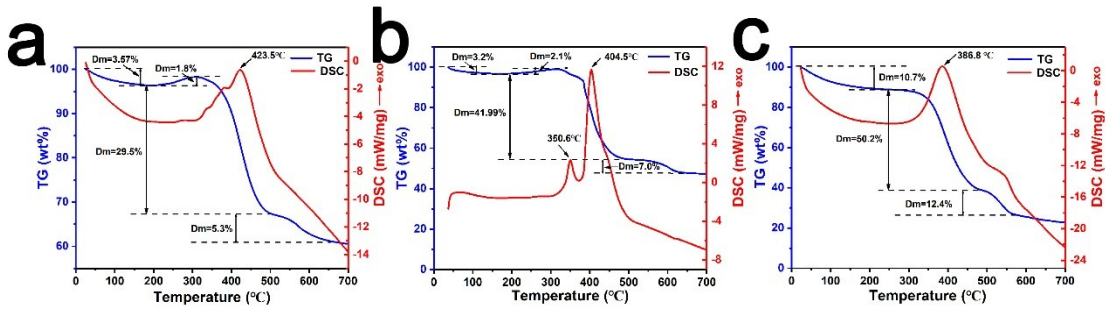

Fig. S8. TG-DSC curve of FS@TO (a), FS (b) and TO (c) heated in air from room temperature to 700 ℃.

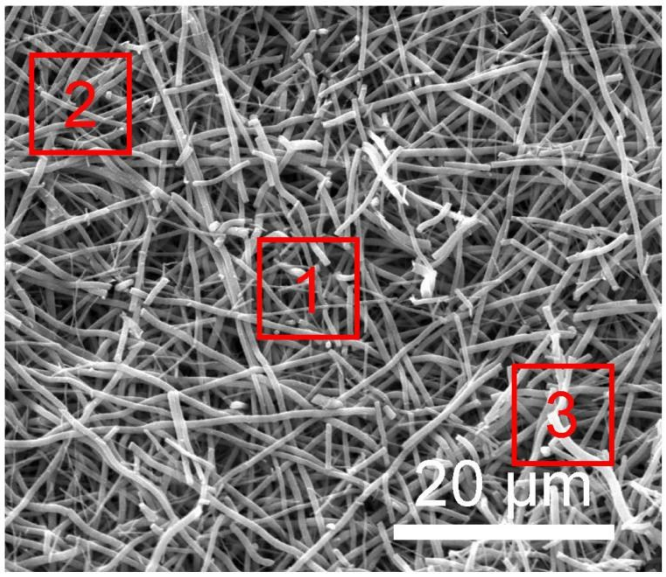

Fig. S9. SEM image and the spots for EDS characterization of FS@TO sample.

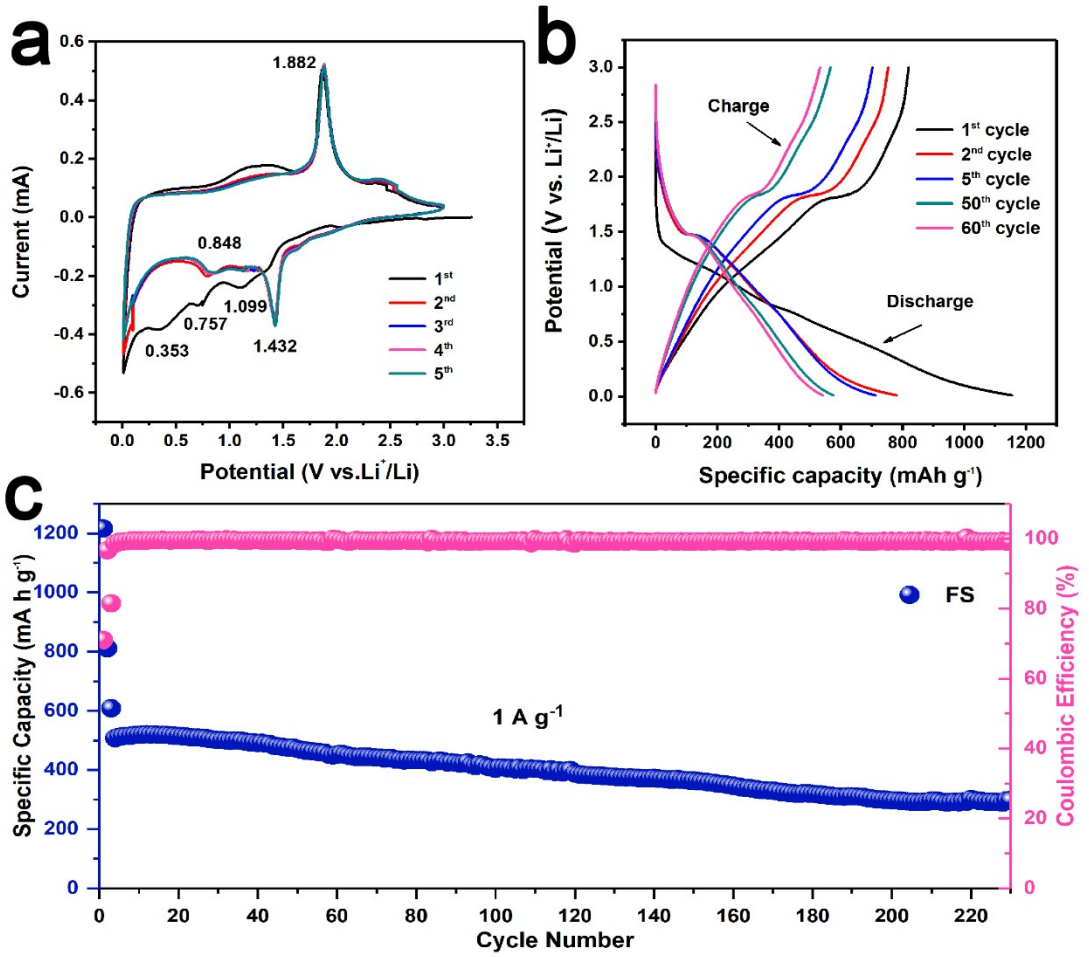

Fig. S10. Electrochemical performance for LIBs: (a) CV curves at 0.1 mV s^{-1} in the voltage range of 0.01-3.0 V versus Li^+/Li (b) the initial, second, fifth, fiftieth and sixtieth discharge/charge profiles of the FS at 0.1 A g^{-1} (c) long cycle performances of the FS at 1.0 A g^{-1}.

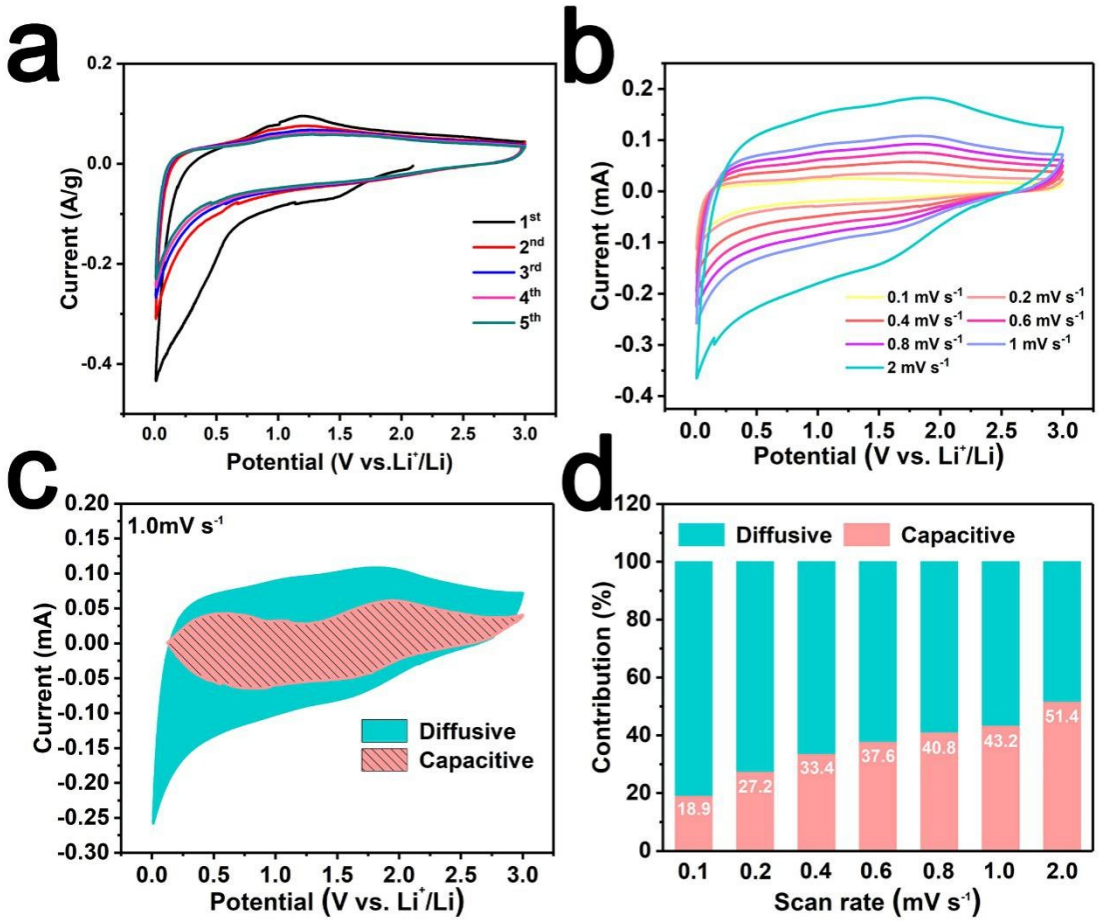

Fig. S11. CV curves of TO sample scaned at 0.1 mV s^{-1} (a) and at different scan rates from 0.1 to 2.0 mV s^{-1} (b), diffusive contribution (mint green) and capacitive contribution (pink) (c) at 1.0 mV s^{-1}, the percentage of pseudocapacitive contribution (d) at different scan rates.

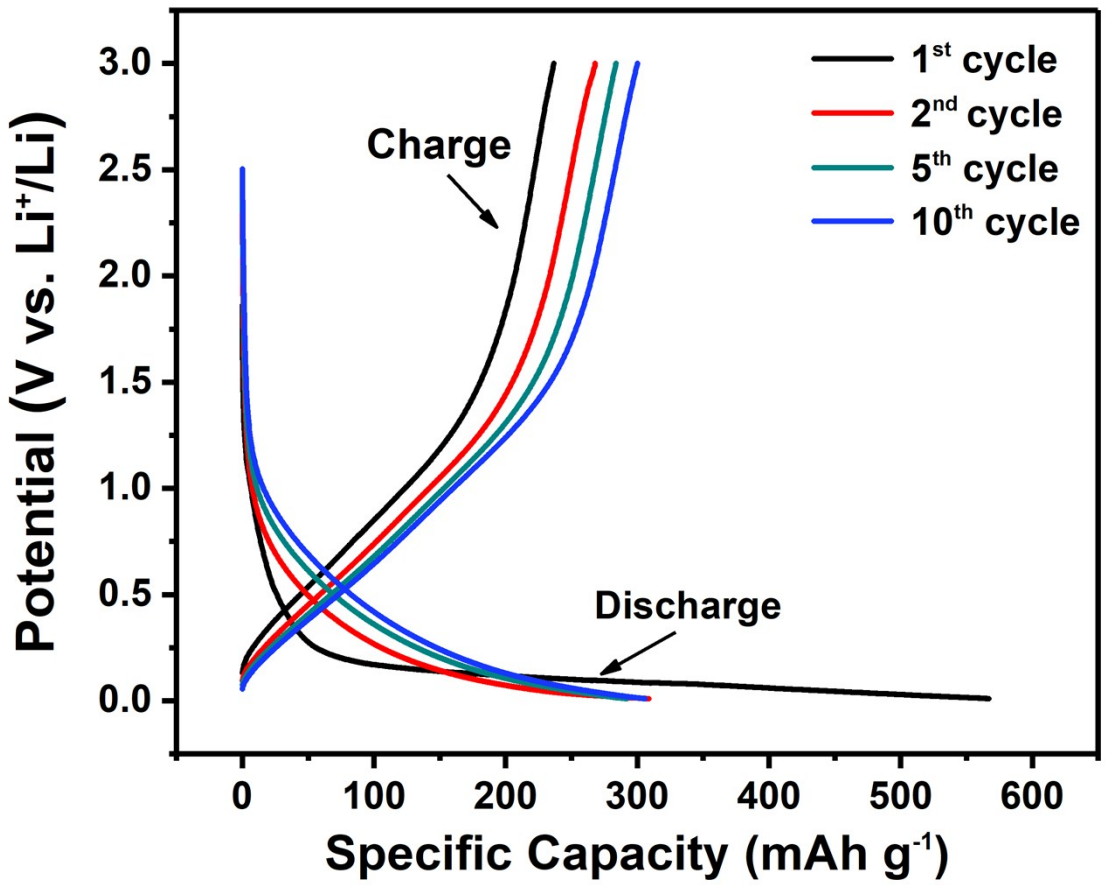

Fig. S12. The initial, second, fifth and tenth discharge/charge profiles of the PVP at 0.1 A g^{-1}.

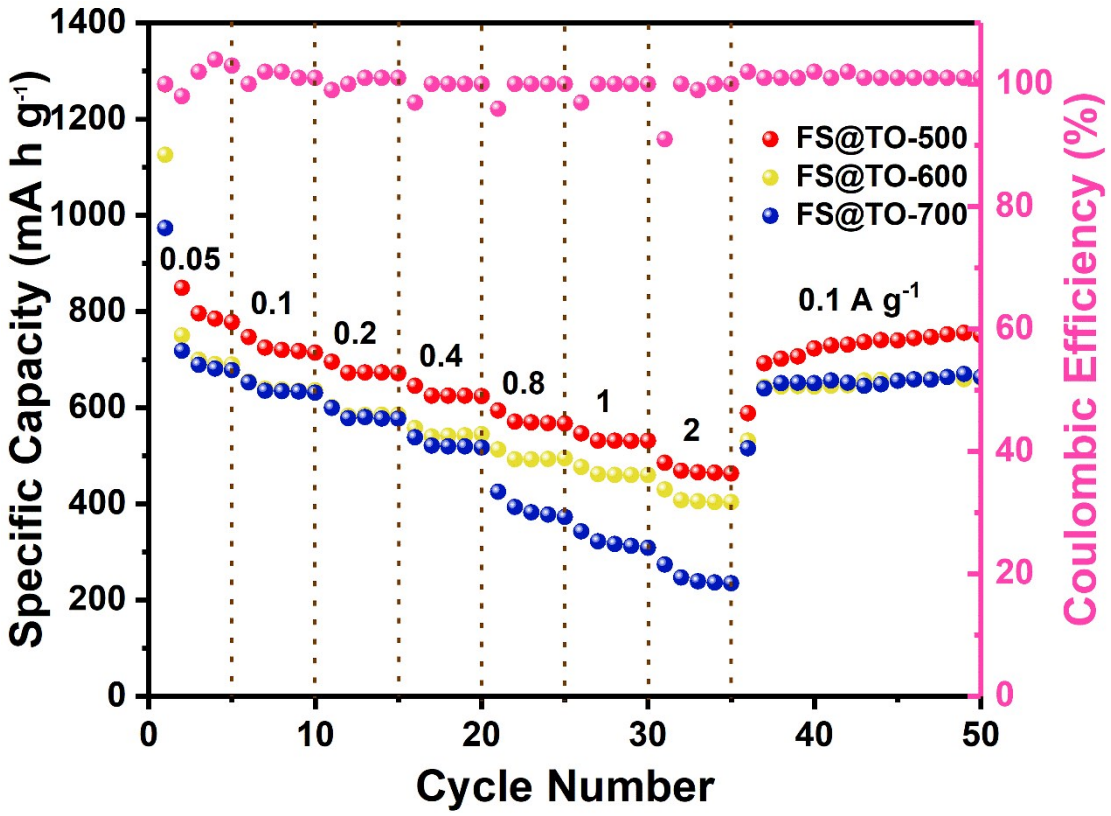

Fig. S13. Rate properties of the FS@TO-500, FS@TO-600, FS@TO-700 at different current densities.

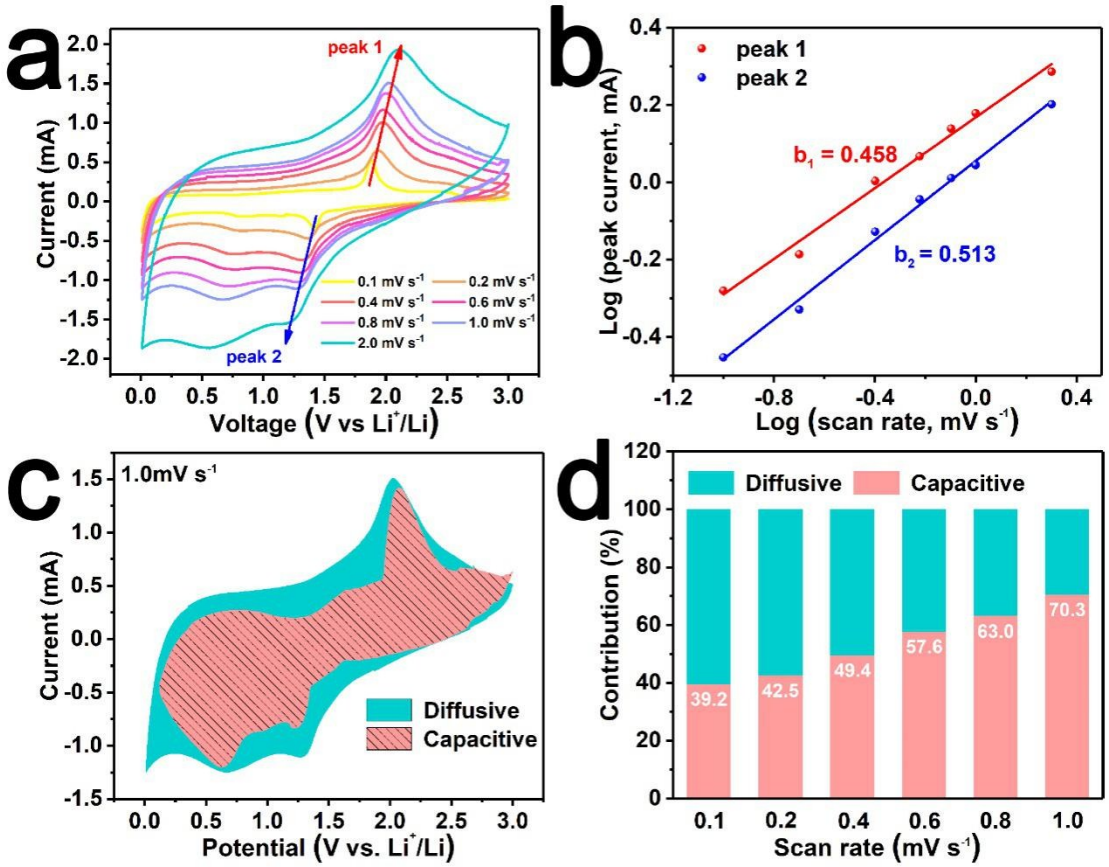

Fig. S14. (a) CV curves at different scan rates from 0.1 to 2.0 mV s^{-1} of the FS; (b) Corresponding log(*I*) versus log(*v*) plots at specific peak currents; (c) Diffusion contribution (mint green) and Capacitive contribution (pink) at 1.0 mV s^{-1}. (d) the percent of pseudocapacitive (diffusion contribution and capacitive contribution) at different scan rates.

The calculation formula for diffusion coefficient based on EIS test is shown as follows [11]:

$$D = \frac{R^2T^2}{2A^2n^4F^4C^2\sigma^2} \qquad \text{Equation S1}$$

Where A represents the surface area of electrode, n means the number of electrons per molecule attending the charge-discharge reaction, F is the Farady constant, C is the concentration of lithium ion in our composite electrode, and σ is the slope of the fitted line Z'-$\omega^{-1/2}$, R represents the gas constant, T is the test temperature.

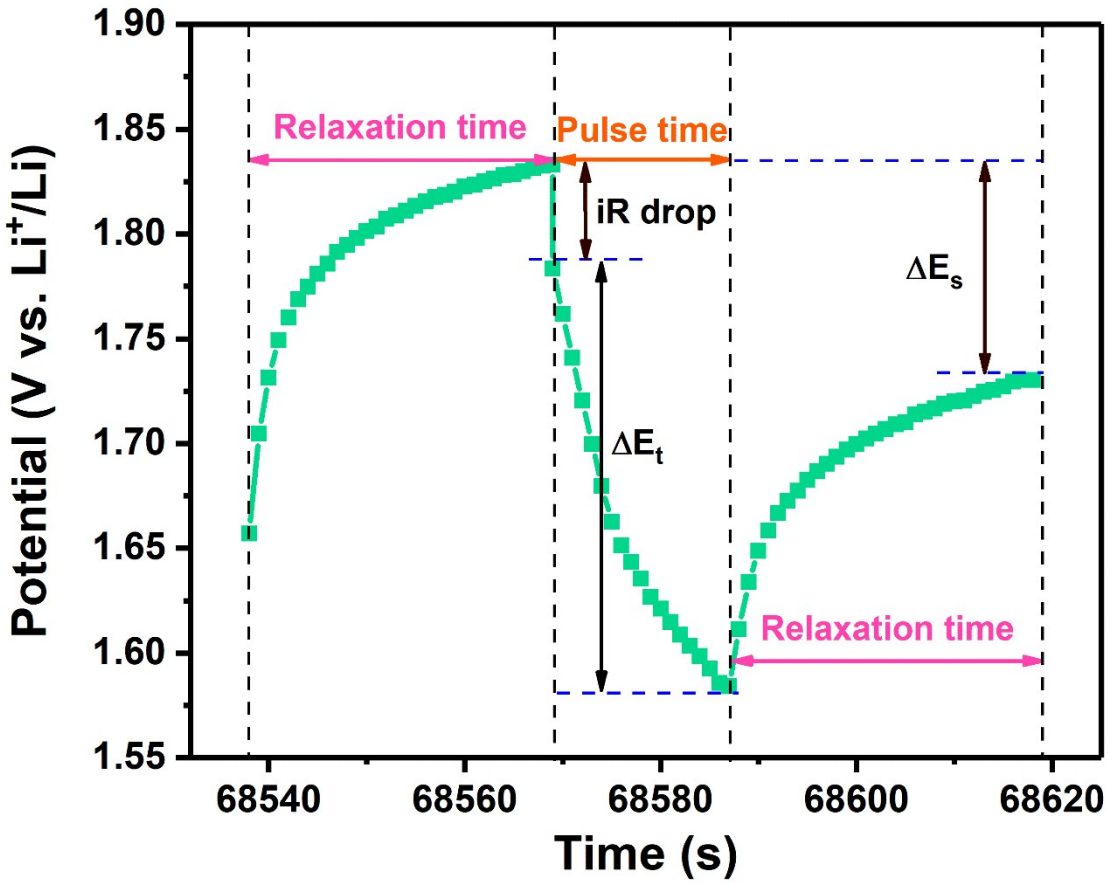

Fig. S15. E vs. t curves of FS@TO electrode for a single GITT during discharge process.

The lithium diffusion coefficient was measured by using Galvanostatic intermittent titration technique (GITT) and calculated based on equation S2 as follows[12].

$$D = \frac{4L^2}{\pi\tau}\left(\frac{\Delta E_s}{\Delta E_t}\right)^2 \qquad \text{Equation S2}$$

Where L is lithium ion diffusion length (unit : cm); for compact electrode, it is equal to average thickness of pole piece measured, τ is the relaxation time (unit : s), and ΔEs is the steady-state potential (unit : V) by the current pluse. ΔEt is the potential change (unit : V) during the constant current pluse after eliminating the iR drop (Fig. S12), τ is the duration of the current pluse (unit : s).

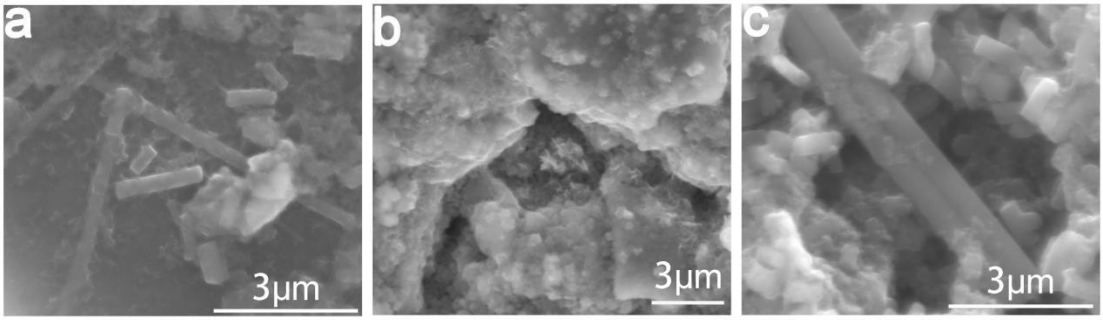

Fig. S16. SEM images of (a) FS@TO (b) FS (c) TO after 50 cycles at 0.5 A g^{-1}.

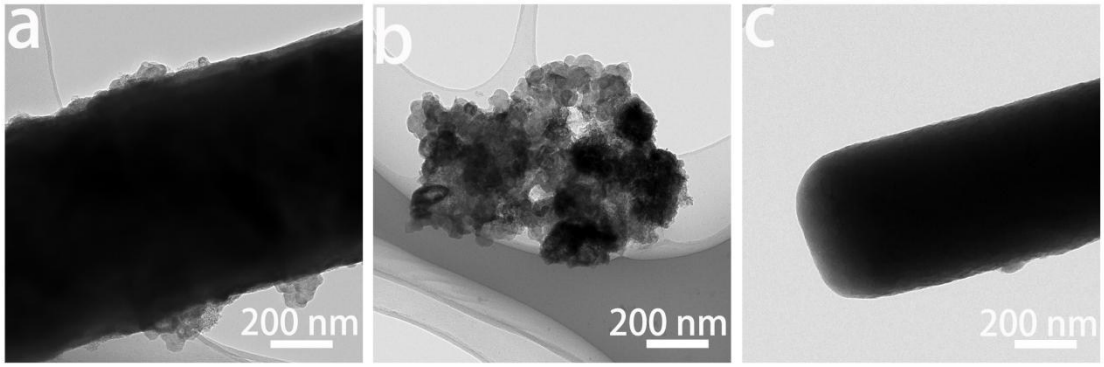

Fig. S17. TEM images of (a) FS@TO, (b) FS and (c) TO after 50 cycles at 0.5 A g^{-1}.

Table S1. Surface area and pore volume analysis results of FS@TO, FS, TO.

Samples	S_{BET} (m^2/g)	$S_{Langmuir}$ (m^2/g)	V_{pore} (cm^3/g)	D_{pore} (nm)
FS@TO	8.1	49.3	0.019	5.8
FS	2.0	7.9	0.006	4.5
TO	12.8	75.4	0.030	5.6

Table S2. C-S analysis result of FS@TO synthesized at 500℃.

Samples	C	S
FS@TO	23.52%	19.44%

Table S3. EDS analysis result of FS@TO sample.

	Element	Fe	Ti	S	C	N	O
Spot 1	**Content (wt%)**	22.62	24.98	10.54	27.32	3.92	10.63
	Content (at%)	9.05	11.66	7.35	50.84	6.26	14.85
Spot 2	**Content (wt%)**	22.64	24.67	10.4	27.22	4.22	10.84
	Content (at%)	9.03	11.47	7.23	50.48	6.71	15.09
Spot 3	**Content (wt%)**	21.28	19.92	9.06	32.3	4.96	12.48
	Content (at%)	7.77	8.48	5.76	54.84	7.23	15.91

Table S4. ICP-OES analysis results of FS@TO nanofibers.

Sample	Element	Content (wt%)	Molar ratio (Fe：Ti)
FS@TO	Fe	16.4%	1 : 1.082
	Ti	15.22%	

According to the TGA results of FS@TO, the mass percentage of the carbonaceous network in FS@TO is about 32.5%. To further confirm the mass percentage of N-doped carbonaceous network, EDS was also employed and results are shown in **Fig. S9** and **Table S3**. The average mass percentage of C and N is about 33.3%, which is consistent with the result obtained from TGA result. **Table S4** shows the test results of ICP-OES, the atom ratio between Ti and Fe is 1.082:1. So the mass ratio between amorphous TiO_2 and FeS is calculated to be 0.983:1. The calculation is based on the equation below:

$$\frac{m_{TiO_2}}{m_{FeS}} = 1.082 * M_{TiO_2}/M_{FeS}$$

where m_{TiO_2} refers to the mass of TiO_2, m_{FeS} refers to the mass of FeS, M_{TiO_2} refers to the molar mass of TiO_2 and M_{FeS} refers to the molar mass of FeS. Thus, the mass percentages of N-doped carbon, amorphous TiO_2 and FeS are around 33.3%, 33.1%, 33.6%, respectively.

Table S5. Comparison of electrochemical performances of FeS-based electrode for lithium-ion batteries.

Electrode description	Voltage window (V)	Rate Capability		Cycling stability		
		Current density (A g^{-1})	Specific capacity (mA h g^{-1})	Current density (A g^{-1})	Cycling numbers (cycles)	Specific capacity (mA h g^{-1})
FeS@TiO_2 [1]	0.01-3.0	0.1/0.5/1	705/474/382	0.2/0.4	100/500	510/430
C@FeS nanosheets [2]	0.01-3.0	0.1/0.5/1/3/6	630/486/425/349/266	0.1	100	615
FeS@rGO [3]	0.01-3.0	0.2/0.5/0.8/1/2/3/5	580/479/433/415/370/339/302	1/5	200/1000	662/325
FeS@C carbon cloth [4]	1.0-2.6	0.15C/0.3C/0.75C/1.5C/7.5C (1C=0.609)	560/530/500/460/370	0.15C/1.2C	100/200	~420/~300
FeS@RGO [5]	0.005-3.0	0.2/0.3/0.5/1	660/530/400/200	0.1/0.3	40/30	978/618
FeS microsheet networks [6]	0.01-3.0	0.1/0.2/0.5/1/2	797/770/505/357/150	0.1	20	697
C/FeS [7]	0.005-3.0	0.5/1/2	485.1/339.4/243.1	2	300	300
G@FeS-GNRs [8]	0.01-3.0	0.1/0.2/0.4/0.8/1	693/600/550/520/498	0.4	100	536
FeS/Ag [9]	0.8-2.5	0.1C/0.5C/1C/2C (1C=0.609)	525/450/200/150			
FeS nanodots in carbon nanowires [10]	1.0-3.0	0.1C/0.5C/1C/2C/5C/10C (1C=609)	579/506/458/422/373/322	0.5C	50	400
This work	**0.01-3.0**	**0.1/0.2/0.4/0.8/1.6/3.2/5**	**804.0/767.8/712.2/654.1/579.4/471.2/359.8**	**0.1/0.5/1**	**100/228/500**	**591/554.6/402.5**

References

[1] X. Wang, Q. Xiang, B. Liu, L. Wang, T. Luo, D. Chen, G. Shen, Sci Rep, 3 (2013) 2007.

[2] C. Xu, Y. Zeng, X. Rui, N. Xiao, J. Zhu, W. Zhang, J. Chen, W. Liu, H. Tan, H.H. Hng, Q. Yan, ACS Nano, 6 (2012) 4713-4721.

[3] M. Huang, A. Xu, H. Duan, S. Wu, Journal of Materials Chemistry A, 6 (2018) 7155-7161.

[4] X. Wei, W. Li, J.A. Shi, L. Gu, Y. Yu, ACS Appl Mater Interfaces, 7 (2015) 27804-27809.

[5] L. Fei, Q. Lin, B. Yuan, G. Chen, P. Xie, Y. Li, Y. Xu, S. Deng, S. Smirnov, H. Luo, ACS Appl Mater Interfaces, 5 (2013) 5330-5335.

[6] C. Xing, D. Zhang, K. Cao, S. Zhao, X. Wang, H. Qin, J. Liu, Y. Jiang, L. Meng, Journal of Materials Chemistry A, 3 (2015) 8742-8749.

[7] J. Zhao, J.A. Syed, X. Wen, H. Lu, X. Meng, Journal of Alloys and Compounds, 777 (2019) 974-981.

[8] L. Li, C. Gao, A. Kovalchuk, Z. Peng, G. Ruan, Y. Yang, H. Fei, Q. Zhong, Y. Li, J.M. Tour, Nano Research, 9 (2016) 2904-2911.

[9] C. Dong, X. Zheng, B. Huang, M. Lu, Applied Surface Science, 265 (2013) 114-119.

[10] C. Zhu, Y. Wen, P.A. van Aken, J. Maier, Y. Yu, Advanced Functional Materials, 25 (2015) 2335-2342.

[11] J.S. Cho, Y.J. Hong, Y.C. Kang, ACS nano, 9 (2015) 4026-4035.

[12] B. Yin, X. Cao, A. Pan, Z. Luo, S. Dinesh, J. Lin, Y. Tang, S. Liang, G. Cao, Advanced Science, 5 (2018) 1800829.